SIK2 and SIK3 differentially regulate mouse granulosa cell response to exogenous gonadotropins in vivo

Emily Hayes, Mariam Hassan, Oliwia Lakomy, Rachael Filzen, Marah Armouti, Marc Foretz, Noriyuki Tsumaki, Hiroshi Takemori, Carlos Stocco

SIK2 and SIK3 differentially regulate mouse granulosa cell response to exogenous gonadotropins *in vivo*.

Emily T. Hayes[1], Mariam Hassan[1], Oliwia Lakomy[1], Rachael Filzen[1], Marah Armouti[1], Marc Foretz[2], Hiromi Takemoto[3], Hiroshi Takemori[4], Carlos Stocco[1]

[1] Department of Physiology and Biophysics, School of Medicine, University of Illinois at Chicago, Chicago, IL 60612

[2] Université Paris Cité, CNRS, INSERM, Institut Cochin, F-75014 Paris, France

[3] Department of Tissue Biochemistry, Graduate School of Medicine and Frontier Biosciences, The University of Osaka, Suita, Osaka 565-0871, Japan

[4] Department of Chemistry and Biomolecular Science, Faculty of Engineering, Gifu University, Gifu 501-1193, Japan

ABSTRACT

Successful development of the ovarian follicle, the functional unit of the ovary, is necessary for normal female fertility, though the molecular mechanisms controlling follicle development remain poorly understood. Salt-inducible kinases (SIKs), a family of serine/threonine kinases, were found to be critical determinants of female fertility. Strikingly, SIK isoforms differentially regulate ovarian function. Thus, SIK2 silencing results in increased ovulatory response to gonadotropins. In marked contrast, SIK3 knockout results in infertility, gonadotropin insensitivity, and ovaries devoid of antral and preovulatory follicles. This study hypothesizes that SIK2 and SIK3 differentially regulate follicle growth and fertility via contrasting actions in the granulosa cells (GCs), the estrogen-producing somatic cells of the follicle. Therefore, SIK2 or SIK3 GC-specific knockdown ($SIK2^{GCKD}$ and $SIK3^{GCKD}$, respectively) mice were generated by crossing SIK floxed mice with *Cyp19a1pII*-Cre mice. Fertility studies revealed that pup accumulation over six months and the average litter size of $SIK3^{GCKD}$ mice are significantly lower compared to controls. Compared to controls, gonadotropin stimulation of prepubertal $SIK2^{GCKD}$ mice results in significantly higher serum estradiol levels, whereas $SIK3^{GCKD}$ mice produced significantly less estradiol. *Cyp11a1, Cyp19a1,* and *StAR* were significantly increased in the GCs of gonadotropin-stimulated mice $SIK2^{GCKD}$. However, *Cyp11a1 and StAR* remained significantly lower than controls in $SIK3^{GCKD}$ mice. Interestingly, *Cyp19a1* stimulation in $SIK3^{GCKD}$ was not statistically different compared to controls. Administering a superovulation regimen to prepubertal mice resulted in $SIK2^{GCKD}$ mice ovulating significantly more oocytes, whereas $SIK3^{GCKD}$ mice ovulated significantly fewer oocytes than controls. Remarkably, $SIK3^{GCKD}$ superovulated ovaries contained significantly more preantral follicles than controls. Finally, immunohistochemistry determination of the apoptosis marker cleaved caspase 3 showed that $SIK3^{GCKD}$ ovaries contained more apoptotic cells than controls. This data points to the differential regulation of GC function and follicle development by SIK2 and SIK3 and supports the therapeutic potential of targeting these kinases for treating infertility or developing new contraceptives.

INTRODUCTION

According to the World Health Organization, infertility is estimated to affect one in six adults worldwide [1]. Of the cases of infertility, 25% are attributed to ovulatory dysfunction [2].

Successful ovulation requires the proper, highly coordinated development of the ovarian follicle, consisting of the oocyte and surrounding steroidogenic somatic cells called granulosa cells (GCs) and theca cells.

The master regulators of the latter half of follicle development and ovulation are the gonadotropins: follicle-stimulating hormone (FSH) and luteinizing hormone (LH) [3]. FSH is produced and released from the pituitary and binds the FSH receptor (FSHR), whose expression in the ovary is restricted to the GCs [4,5]. FSHR is a Gs-coupled protein receptor and thus triggers downstream signaling cascades, including the canonical cAMP/PKA/CREB pathway [6]. FSHR activation stimulates GC proliferation and steroidogenic gene expression needed to produce estradiol and progesterone [7]. However, the mechanisms governing normal follicle development and the perturbations in these pathways that lead to infertility are incompletely understood.

Recently discovered players in the regulation of fertility in the ovary include the salt-inducible kinases (SIKs). The SIKs, consisting of SIK1, SIK2, and SIK3, are a family of AMPK-related serine-threonine kinases with well-established roles as crucial regulators of cAMP-, PKA-, and CREB-mediated signaling pathways [8]. Our group was the first to demonstrate the critical roles of SIK2 and SIK3 in female fertility [9]. We demonstrated that global SIK2 knockout (SIK2KO) mice have an enhanced ovulatory response to a superovulation protocol, ovulating approximately three times as many oocytes as wild-type controls. In contrast, SIK3KO mice are infertile, do not ovulate in response to exogenous gonadotropin stimulation, and lack large antral follicles in their ovaries. Furthermore, we showed that broad inhibition of the SIKs with small molecule inhibitors in rat and human GCs and targeted knockdown of SIK2 in rat GCs potentiates FSH-induced transcription of steroidogenic genes [9]. Mechanistically, the potentiation of FSH-induced gene expression in rat GCs caused by SIK inhibition is likely through modulating the cellular localization of CREB-regulated transcriptional coactivator 2 (CRTC2) [10], a well-characterized target of SIK phosphorylation.

Because global knockout mice of the SIKs revealed that SIK2 and SIK3 are involved in follicle development and fertility and that SIK inhibition *in vitro* enhances GC steroidogenesis [9,10], we hypothesized that SIK2 and SIK3 are crucial for normal GC function and, therefore, needed for ovulation and female fertility. To test this hypothesis, we developed SIK2 and SIK3 GC-specific knockdown mice, characterized their reproductive phenotypes, and determined the effect of loss of SIK2 or SIK3 on steroidogenesis, proliferation, and apoptosis in GCs *in vivo*. Further understanding the roles of SIK2 and SIK3 in the ovary will provide mechanistic insight into the regulation of ovarian fertility and may shed light on the potential of the SIKs to be targeted for treating infertility or developing new contraceptive strategies.

METHODS

Animals

Animals were treated following the National Institutes of Health Guide for the Care and Use of Laboratory Animals. All protocols were approved by the University of Illinois at Chicago Animal Care Committee. Mice were housed at the University of Illinois at Chicago Biologic Resources Laboratory under constant temperature, humidity, and light (14 h light/10 h dark) with free access to food and water. All transgenic mice were on a C57BL/6J background. Mice containing LoxP sites flanking exon 5 of the SIK2 or SIK3 genes ($SIK2^{flox/flox}$ and $SIK3^{flox/flox}$) were obtained from Marc Foretz [11] and Hiromi Takemoto [12]. Global genomic knockout of SIK2 alleles was generated by crossing $SIK2^{flox/flox}$ mice with transgenic *Zp3*-Cre mice (Jackson

Laboratory, Bar Harbor, ME). $SIK2^{flox/-}$ or SIK3 floxed mice were bred with mice expressing cre-recombinase driven by the CYP19A1 (aromatase) proximal promoter II (Cyp19-Cre). The CYP19A1 proximal promoter II is active exclusively in the GCs in the ovary in adult mice in follicles transitioning from the preantral to the preovulatory stage [13]. However, it is low or undetectable in GCs of primordial primary and secondary follicles, theca cells, and oocytes. Cyp19pII-cre mice were obtained from Joanne Richards [13]. Therefore, the genotype of $SIK2^{GCKD}$ mice is $SIK2^{flox/-}$;Cyp19-Cre and that of $SIK3^{GCKD}$ mice is $SIK3^{flox/flox}$;Cyp19-Cre. Wild-type controls were functionally wild-type littermates of the mice with the desired experimental genotypes.

Fertility studies

Control and experimental female mice (30-65 days old) were continuously paired with male mouse breeders for six months. Breeding cages were checked weekly and litters produced by each breeding pair were counted for the number of pups and recorded. The number of pups accumulated by the end of each month of breeding was calculated for each female breeder, and then the mean number of pups accumulated by the end of each pup was calculated for each genotype. The mean litter size of each genotype was calculated.

Granulosa cell isolation

Prepubertal (D21-30) mice were stimulated with 5 IU eCG (Calbiochem, Cat. No. 367222, San Diego, CA) via intraperitoneal injection. Forty-eight hours later, mice were sacrificed, and ovaries were harvested and placed in ice-cold phosphate-buffered saline (PBS). Ovaries were cleaned of surrounding tissue and then placed in 1 mL of fresh ice-cold PBS. Large antral follicles were gently expressed for 1-2 minutes using two 25-gauge needle syringes to release GCs. The residual ovaries were discarded, and the PBS containing GCs was filtered through a 40 μm cell strainer (Greiner, Monroe, NC) to remove oocytes. After that, the cells were centrifuged at 4 degrees Celsius for 3 minutes at 3,000 rpm, and then the PBS was aspirated from the cell pellet. The cell pellets were stored at -80 degrees Celsius until total RNA isolation.

RNA isolation and quantification

Total RNA was isolated from GCs using TRIzol (Invitrogen, Carlsbad, CA) following manufacturer's instructions. cDNA was made by reverse transcribing 0.5 μg total RNA using anchored oligo-dT primers (Integrated DNA Technologies, Coralville, IA) and Moloney Murine Leukemia Virus reverse transcriptase (Genscript, Piscataway, NJ). To measure gene expression, intron-spanning primers (Table 1) were designed to amplify each gene of interest, and then the copy number was determined using a standard curve consisting of a serial dilution of the PCR product for each gene of interest. For measuring Sik2 and Sik3, intron-spanning primers were designed such that either the forward or reverse primer was specific to exon 5 of the gene, which is removed upon recombination by Cre recombinase. Gene expression was normalized to the copy number of one of two housekeeping genes: ribosomal protein L19 (*Rpl19)* or TATA-box binding protein (*Tbp*).

Gene of interest	Primer sequences
Rpl19	Forward: 5'-GTA TCA CAG CCT GTA CCT GA-3' Reverse: 5'-GGA AGC TTT ATT TCT TGG TC-3'
Tbp	Forward: 5'-AGG AGA TAT TCA GAG GAT GC-3'

	Reverse: 5'-CTG TTG GTG TTC TGA ATA GG-3'
Cyp19 a1	Forward: 5'-ATT GCA GCC CCT GAC ACC AT-3' Reverse: 5'- TGG CGA TGT ACT TCC CAG CA-3'
Cyp11 a1	Forward: 5'-GAT GTT CCA CAC CAG TGT CCC-3' Reverse: 5'-AGG GTA CTG GCT GAA GTC TCG C-3'
StAR	Forward: 5'-TTT TGG GGA GAT GCC GGA GC-3' Reverse: 5'-GCG AAC TCT ATC TGG GTC TGC G-3'
Sik1	Forward: 5'-GGG AGT TCG GAC GGA GGA CT-3' Reverse: 5'-GCA CAG CCG TCT TAC CTC CC-3'
Sik2	Forward: 5'-CTT TAA AAC TGG TGA ACT GC-3' Reverse: 5'-TAC AGG AAC CTC TAT GAG CA-3'
Sik3	Forward: 5'-CAG CAA CCT CTT CAC TCC-3' Reverse: 5'-CTT TCC TCC TTC AGT TGC-3'

Immunoblotting

Protein was isolated from GCs using RIPA buffer (Sigma, St. Louis, MO) containing Halt Protease Inhibitor Cocktail and Halt Phosphatase Inhibitor Cocktail (Thermo Scientific, Waltham, MA). Protein concentration was determined using the Pierce BCA Protein Assay Kit (Thermo Scientific, Waltham, MA). Thereafter, 10 ug of protein from each sample was denatured and separated using Bis-Tris polyacrylamide (12%) gel electrophoresis. Proteins were transferred to an Immobilon-P PVDF Membrane (Millipore, Burlington, MA). The membrane was blocked for one hour at room temperature using 5% milk in Tris-buffered saline, 0.1% Tween 20 (TBST), then incubated overnight in primary antibody diluted in 1% bovine serum albumin (BSA) in TBST. The primary antibodies used were SIK2 (1:1000, Cell Signaling Technology, Cat. No. 6919, Danvers, MA), SIK3 (1:2000, LS Bio, Cat. No. LS-B15472, Shirley, MA), and GAPDH (1:10000, ProteinTech, Cat. No. 60004-1-Ig, Rosemont, IL). Membranes were washed with TBST and then subjected to a one-hour incubation at room temperature with secondary antibodies diluted 1:5000 in 5% milk in TBST. The secondary antibodies used were horseradish peroxidase-conjugated goat anti-mouse IgG (Jackson Immunoresearch, Cat. No. 115-035-003, West Grove, PA) and goat anti-rabbit IgG (Jackson Immunoresearch, Cat. No. 111-035-003, West Grove, PA). Membranes were washed with TBST, then proteins were visualized using SuperSignal West Pico PLUS or SuperSignal West Femto Maximum Sensitivity Substrate enhanced chemiluminescent (ECL) substrate (Thermo Scientific, Waltham, MA) and imaged on a Chemidoc MP Imaging System (Bio-Rad, Hercules, CA).

Superovulation

Prepubertal (D21-28) mice were stimulated with 5 IU equine chorionic gonadotropin (eCG) (Calbiochem, Cat. No. 367222, San Diego, CA) via intraperitoneal (IP) injection. Forty-eight hours later, mice were stimulated with 5 IU human chorionic gonadotropin (hCG) (Calbiochem, San Diego, CA) via IP injection. Seventeen hours later, mice were sacrificed, and the intact ovaries and oviducts were harvested. Cumulus-oocyte complexes were released from the ampulla and were counted using a dissection scope.

Measuring oocytes ovulated in unstimulated mice

Reproductive-age mice (6-8 weeks old) were given daily vaginal lavages at 3:00 PM to track their estrus cycles. Vaginal lavage was performed using 10 ul PBS to wash the vaginal opening 10-20 times. The lavage sample was smeared on a microscope slide and fully dried. Thereafter,

slides were submerged in 0.1% crystal violet (Sigma, Cat. No. C0775, St. Louis, MO) for 1 minute, then washed with dH2O for 1 minute and allowed to dry. Using brightfield microscopy at 10X, cytology was assessed to determine the estrus cycle stage based on established criteria [14]. When mice were determined to be in the proestrus stage in the afternoon, it was anticipated that the mice would begin and complete ovulation by 11:00 AM the following day [15]. At 11:00 AM the following morning, mice were sacrificed, and the intact ovaries and oviducts were harvested. Cumulus-oocyte complexes were released from the ampulla and were counted using a dissection scope for visualization.

Immunohistochemistry

Ovaries were fixed overnight at 4 degrees Celsius in modified Davidson's fixative and stored in 75% ethanol at 4 degrees Celsius before paraffin embedding. 5 µm sections were deparaffinized and rehydrated. Antigen retrieval was performed by gently boiling slides in 1 mM EDTA, 0.5% Tween 20 (pH 8.0) for 3 minutes in a microwave, allowing to cool, then repeating for an additional 3 minutes. Sections were blocked for one hour at room temperature in 5% BSA in permeabilization buffer (0.2% w/v gelatin, 0.2% v/v triton in PBS) and then incubated overnight at 4 degrees Celsius in primary antibody diluted in 1% BSA in permeabilization buffer. The primary antibodies used were SIK2 (1:500, LS Bio, Cat. No. LS-B2068, Shirley, MA), Cleaved Caspase-3 (1:500, Cell Signaling Technology, Cat. No. 9661S, Danvers, MA), and proliferating cell nuclear antigen (PCNA) (1:2000, ProteinTech, Cat. No. 60097-1-Ig, Rosemont, IL). Slides are washed in 0.1% Tween 20 in PBS (PBST) and then incubated in secondary antibody diluted 1:400 in 1% BSA in permeabilization buffer. The secondary antibodies used were horseradish peroxidase-conjugated goat anti-mouse IgG (Jackson Immunoresearch, Cat. No. 115-035-003, West Grove, PA) and goat anti-rabbit IgG (Jackson Immunoresearch, Cat. No. 111-035-003, West Grove, PA). Slides were washed in PBST and then exposed to DAB substrate (Vector, Cat. No. SK-4100, Newark, CA) for 2 minutes. Sections were counterstained with hematoxylin from the Hematoxylin and Eosin Stain Kit (Vector, Cat. No. H-3502, Newark, CA). Sections were dehydrated, cleared, and mounted using Cytoseal (Epredia, Portsmouth, NH).

Quantifying proliferation and apoptosis

Ovary sections stained via IHC for cleaved caspase 3 and PCNA were imaged with a 10X objective on a Nikon Eclipse Ti2E Inverted Microscope (Nikon, Tokyo, Japan) using identical brightfield settings. These images of whole ovary sections were opened in ImageJ software, version 1.54f (National Institutes of Health, USA). Using the “Colour Deconvolution” function, images were separated into brown and blue channels, representing DAB and hematoxylin, respectively. Next, using the "Threshold" function, the maximum threshold was set to select only the dark brown DAB-positive cells for cleaved caspase-3, and only the distinct brown nuclei for PCNA, and this threshold number was kept constant between images. The ovary was selected using the "Freehand selections" tool, then the DAB-positive pixels and area of the ovary were quantified using the "Measure" function. The sum of the values of the pixels within the selection (RawIntDen) was divided by the area of the ovary and compared between genotypes. One middle section was analyzed per ovary.

H&E and follicle counts

Serial 5 µm sections were deparaffinized, rehydrated, and then stained using the Hematoxylin and Eosin Stain Kit (Vector, Cat. No. H-3502, Newark, CA) following manufacturer's instructions. Every tenth section was visualized using a 10X objective on a

brightfield microscope, and follicles were counted. Only follicles with the oocyte nucleus visible in the section were counted. Follicles were classified as "secondary" if the oocyte was surrounded by 5 or more layers of GCs without any antrum formation, as "early antral" if there were several small cavities scattered throughout the granulosa cell layers, as "antral" if there was one fluid-filled antrum but no cumulus stalk, and as "preovulatory" if there was one large antrum and a well-formed cumulus stalk, as previously described [16]. Ten sections from one ovary per animal were counted. Follicle numbers for each animal were multiplied by 10 to account for counting $1/10^{th}$ of the total sections in the ovary. To correct for the size of the ovary, follicle numbers were then normalized to the relative number of sections per ovary. Corpora lutea, characterized by GCs with a hypertrophied, lighter-stained appearance, were counted in two middle sections at least 200 μm apart per ovary. The mean number of follicles per follicle type was compared between genotypes.

Estradiol measurement

eCG-stimulated prepubertal animals were anesthetized, and blood was collected via cardiac puncture using a 25-gauge needle. Blood was incubated at room temperature for 30-60 minutes and then centrifuged at 4 degrees Celsius for 10 minutes at 1.5 RCF. Thereafter, sera was removed and stored at -80 degrees Celsius. Undiluted serum was subjected to an estradiol ELISA (DRG International, Springfield, NJ) in accordance with the manufacturer's instructions.

Statistics

Data were analyzed using Prism 6 (GraphPad, Boston, MA). Differences between two groups were determined by Student's t-test. Differences between multiple groups were determined by one-way ANOVA with Tukey's post-hoc test. To compare pups accumulated over time between genotypes, significant differences were determined by repeated measures ANOVA. To compare follicle counts of each follicle type between genotypes, significant differences were determined by two-way ANOVA with Bonferroni post hoc test. Data are represented as mean +/- SEM. Significant differences were recognized at $P<0.05$.

RESULTS

To evaluate the reproductive effects of SIK2 or SIK3 loss in GCs, we developed SIK2 and SIK3 GC-specific knockdown mouse models (referred to hereon as $SIK2^{GCKD}$ and $SIK3^{GCKD}$, respectively) using the Cre-loxP system. Mice carrying floxed exon 5 of the SIK2 or SIK3 genes were previously described [11,12]. Floxed mice were crossed with transgenic mice containing the Cre recombinase gene downstream of the Cyp19a1 proximal promoter II (Cyp19a1pII-Cre), which is active specifically in the GCs of follicles between the preantral and preovulatory stages [13]. Because the Cyp19a1 pII promoter is activated by the gonadotropins, the experimental design utilized here was to stimulate prepubertal mice with equine chorionic gonadotropin (eCG) for 48 hours to stimulate follicle growth as well as Cre recombinase expression.

To validate the $SIK2^{GCKD}$ and $SIK3^{GCKD}$ mouse models, ovaries were harvested from eCG-stimulated mice, and then GCs were isolated to quantify SIK mRNA and protein levels (Figure 1). $SIK2^{GCKD}$ GCs had significantly less *Sik2* expression than controls, with no significant changes in *Sik1* or *Sik3* expression (Figure 1A). Further, $SIK2^{GCKD}$ GCs showed little to no SIK2 protein expression compared to wild types (Figure 1B). Unexpectedly, $SIK2^{+/-}$ GCs showed a visible reduction in SIK2 protein expression, suggesting possible haploinsufficiency of SIK2. $SIK3^{GCKD}$ GCs had significantly decreased expression of *Sik3* compared to controls, whereas there was no significant change in *Sik1* or *Sik2* expression (Figure 1C). This corresponded with

a visible reduction in SIK3 protein expression compared to controls (Figure 1D). Interestingly, both SIK2^{GCKD} and SIK3^{GCKD} GCs showed a trend toward increased *Sik1* expression (Figure 1A). Together, this data shows that a significant knockdown of *Sik2* or *Sik3* mRNA and protein levels was achieved in GCs.

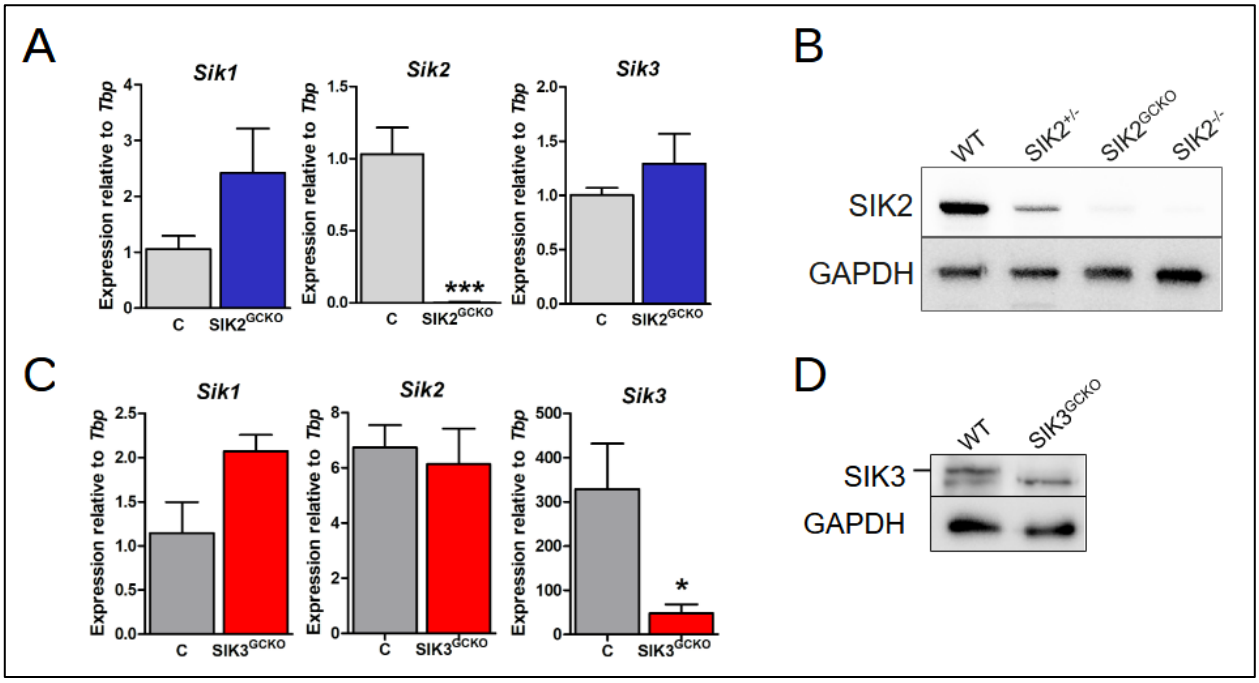

Figure 1. Measurement of SIK knockdown in SIK2^{GCKD} and SIK3^{GCKD} GCs. Prepubertal (21-30 days old) mice were stimulated with 5 IU eCG for 48 hours, then GCs were harvested, and total RNA and protein were isolated. (**a, c**) Expression of *Sik1*, *Sik2*, and *Sik3* was measured relative to *Tbp* by quantitative qPCR in wild-type control (C) versus SIK2^{GCKD} (**a**) or SIK3^{GCKD} (**c**) GCs (n=3). (**b**) Protein levels of SIK2 and GAPDH in wild-type (WT), SIK2$^{+/-}$, SIK2^{GCKD}, and SIK2$^{-/-}$ GCs (n=3). (**c**) Protein levels of SIK3 and GAPDH in WT and SIK3^{GCKD} GCs (n=2). Values are displayed as the mean +/- SEM. Statistical significance was determined by Student's t-test. *P<0.05; ***P<0.001 vs. controls.

To determine the effects of the loss of SIK2 and SIK3 in GCs on fertility, reproductive-age females were bred for six months and their litters were tracked (Figure 2). SIK2^{GCKD} animals had a similar litter size compared to wild-type controls, while SIK3^{GCKD} animals showed a significant decrease in litter size (Figure 2A). Similarly, SIK2^{GCKD} animals accumulated a similar number of pups over six months compared to controls, whereas SIK3^{GCKD} breeders accumulated significantly fewer pups (Figure 2B), likely due to significantly smaller litter sizes (Figure 2A). Thus, this suggests that SIK2^{GCKD} did not affect normal fertility, whereas SIK3^{GCKD} resulted in subfertility.

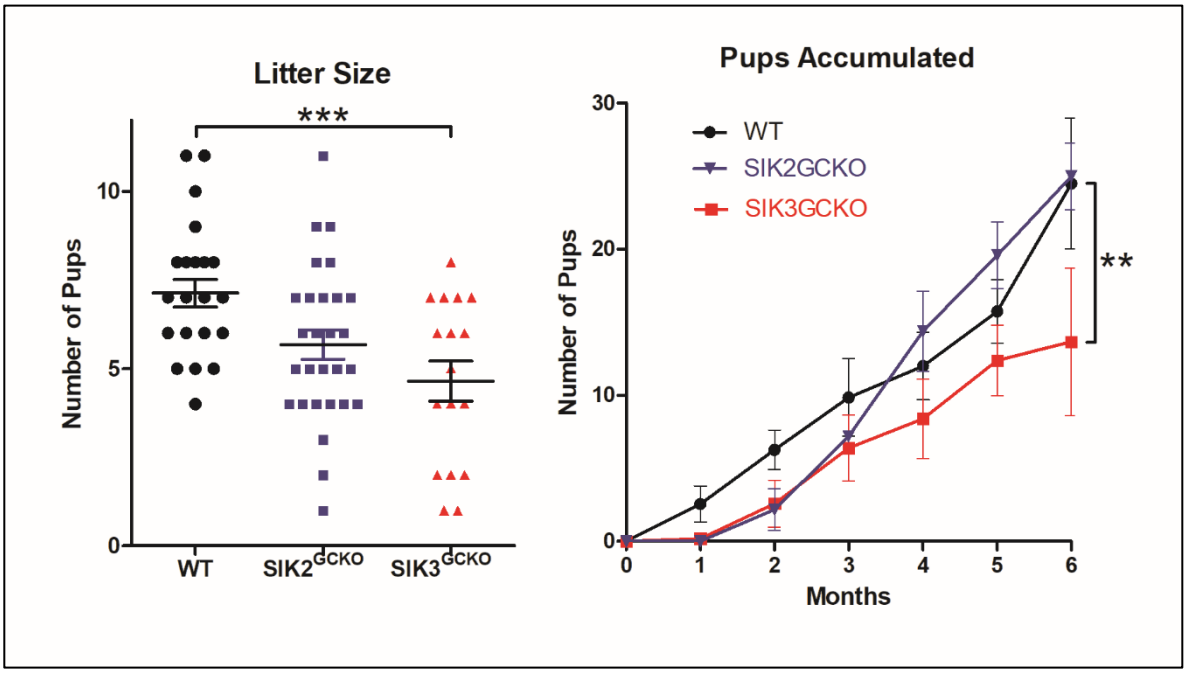

Figure 2. Determining the effect of the loss of SIK2 and SIK3 in GCs on female fertility. Reproductive-age (30-65 days old) female mice were continuously paired with a male breeder for 6 months, and the litters were tracked. (**a**) The number of pups per litter was recorded for each litter and compared between wild-type controls (WT), SIK2^{GCKD}, and SIK3^{GCKD} female breeders. Error bars represent the mean +/- SEM. Statistical significance was determined by one-way ANOVA. (b) The total number of pups accumulated by the end of each month of continuous breeding was calculated for WT (*n*=7), SIK2^{GCKD} (*n*=5), and SIK3^{GCKD} (*n*=5) female breeders. Values are displayed as the mean +/- SEM. Statistical significance was determined by repeated measures ANOVA. **P*<0.05; ****P*<0.001 vs. WT.

One of the main functions of ovarian follicles is to produce estradiol to support female fertility. To investigate whether estradiol production is altered in the GC knockdowns, sera from eCG-stimulated animals were collected, and estradiol concentration was measured (Figure 3). SIK2^{GCKD} sera contained significantly more estradiol than controls (Figure 3A). In contrast, SIK3^{GCKD} animals had significantly less serum estradiol (Figure 3B), suggesting a possible mechanism by which the loss of SIK3 in GCs resulted in subfertility (Figure 2).

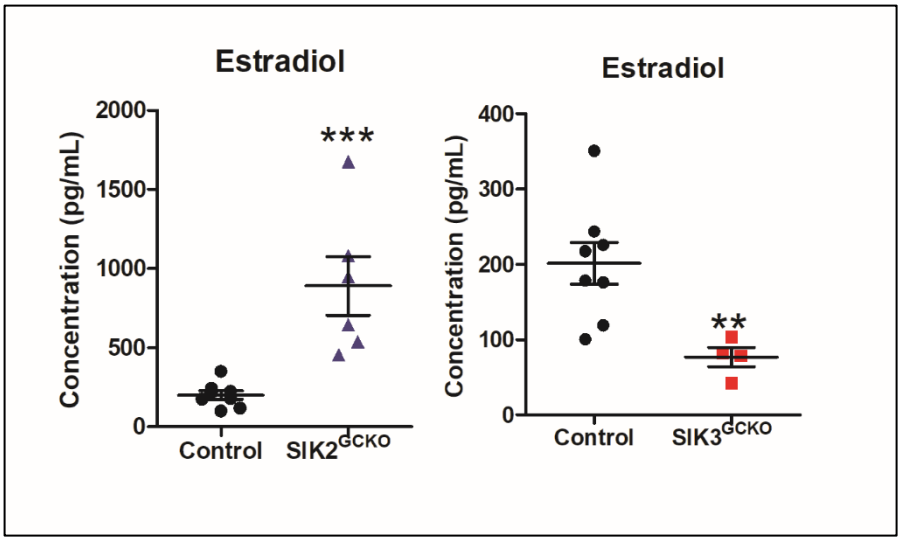

Figure 3. Loss of SIK2 and SIK3 in GCs differentially regulated serum estradiol. Prepubertal (21-30 days old) mice were stimulated with 5 IU eCG for 48 h, then serum was collected to measure estradiol concentration via ELISA in wild-type (Control) vs. $SIK2^{GCKD}$ (left) and $SIK3^{GCKD}$ (right) mice. Error bars represent the mean +/- SEM. Statistical significance was determined by Student's *t*-test. ***P*<0.01; ****P*<0.001 vs. Control.

The differential effect of SIK2 or SIK3 knockdown in fertility and estradiol levels led to the hypothesis that SIK2 and SIK3 differentially regulate the expression of steroidogenic enzymes involved in the production of estradiol, including steroidogenic acute regulatory protein (StAR), cholesterol side-chain cleavage enzyme (P450scc, encoded by *Cyp11a1*), and aromatase (encoded by *Cyp19a1*). Thus, gene expression was measured in the GCs of eCG-stimulated animals (Figure 4). In concordance with the serum estradiol data (Figure 3), $SIK2^{GCKD}$ showed significantly increased steroidogenic gene expression of *Star*, *Cyp11a1*, and *Cyp19a1* (Figure 4A), whereas $SIK3^{GCKD}$ showed significantly decreased gene expression of *Star* and *Cyp11a1*. Strikingly, the knockdown of SIK3 only tended to decrease in *Cyp19a1* expression, suggesting that SIK3 may indirectly regulate estradiol production (Figure 4B). The data indicates that SIK2 may directly regulate estradiol production in GCs via steroidogenic gene expression. In contrast, although SIK3 knockdown also decreased the expression of steroidogenic genes, it appears that this effect is indirect, at least at the level of estradiol production.

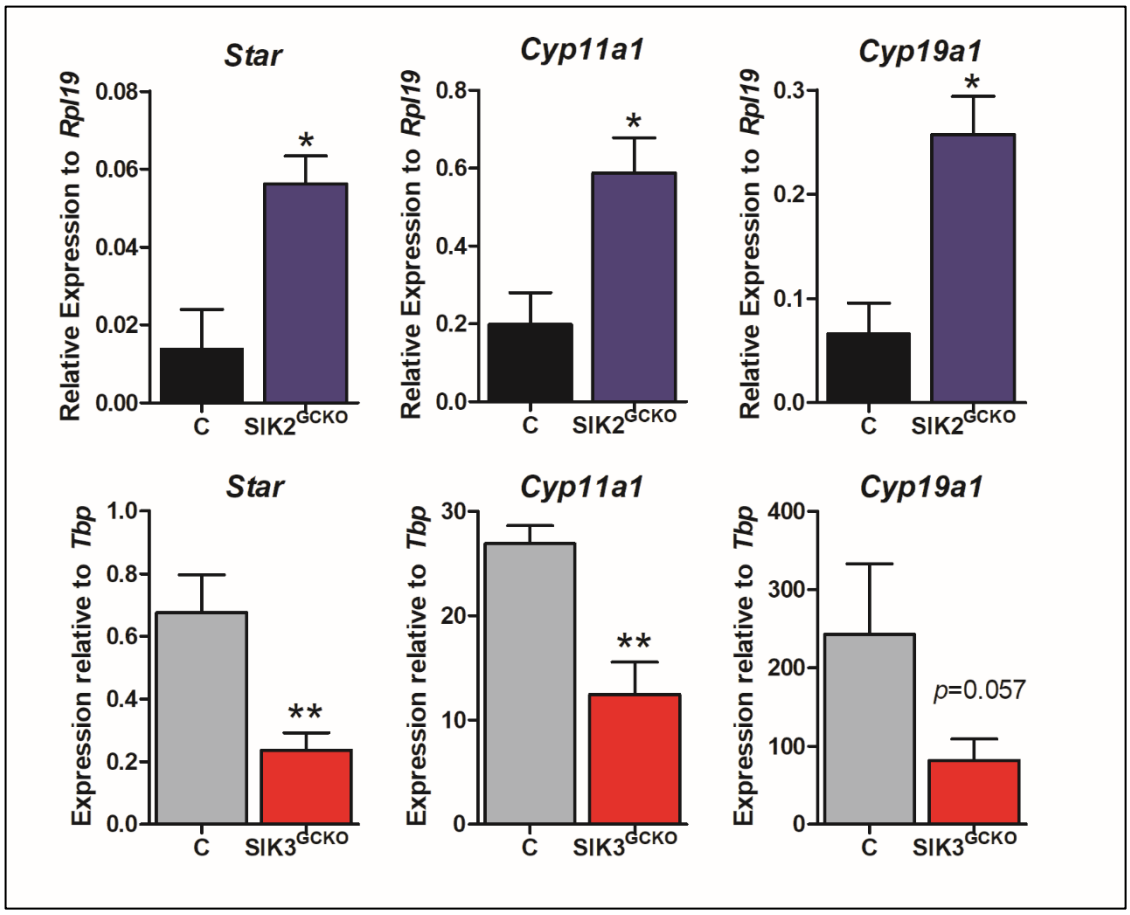

Figure 4. SIK2 and SIK3 differentially regulate steroidogenic gene expression in GCs. Prepubertal (21-30 days old) mice were stimulated with 5 IU eCG for 48 h, then GCs were isolated and total RNA was harvested. Expression of *Star*, *Cyp11a1*, and *Cyp19a1* was measured relative to *Rpl19* (top) or *Tbp* (bottom) by quantitative qPCR in wild-type controls (C) versus SIK2^{GCKD} (top) or SIK3^{GCKD} (bottom) GCs (*n*=3). Values are displayed as the mean +/- SEM. Statistical significance was determined by Student's *t*-test. **P*<0.05; ***P*<0.01; ****P*<0.001 vs. controls.

Estradiol is essential for promoting follicle growth to the preovulatory stage. Therefore, it was hypothesized that the alterations in estradiol seen in the SIK2^{GCKD} and SIK3^{GCKD} animals impact follicle development and ovulation. Therefore, we next subjected mice to a superovulation protocol, and then the number of oocytes ovulated was counted in the ampulla of the oviduct (Figure 5A). SIK2^{GCKD} mice ovulated significantly more oocytes than controls (Figure 5A). Because gonadotropin-stimulated SIK2^{GCKD} and SIK2^{KO} mice have increased ovulation but unstimulated SIK2^{GCKD} mice have average litter sizes (Figure 2A), the number of oocytes ovulated under physiologic conditions was counted in unstimulated SIK2KO mice the morning after proestrus (Figure 5B). Interestingly, SIK2^{KO} animals ovulated a similar number of oocytes compared to controls (Figure 5B). Thus, this hyper-fertile response in SIK2^{GCKD} was only seen with supraphysiologic levels of gonadotropins.

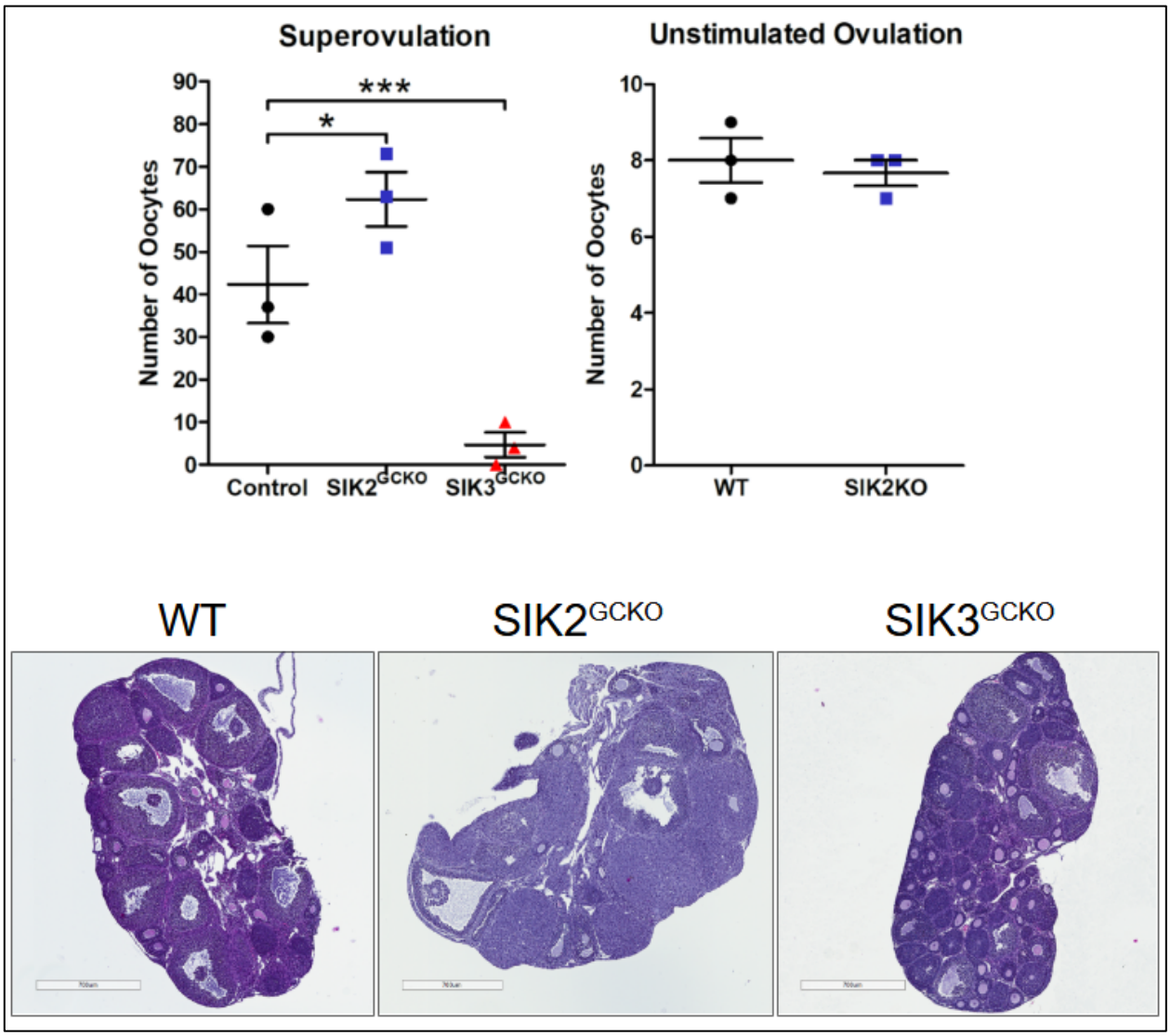

Figure 5. SIK2 and SIK3 in GCs differentially regulate ovulatory response to superovulation. (a) Prepubertal (21-30 days old) mice were stimulated with 5 IU eCG for 48 h followed by 5 IU hCG for 17 h to stimulate ovulation. Thereafter, oocytes were counted in the ampulla of each oviduct. The total number of oocytes ovulated by each animal is shown for wild-type controls (WT), SIK2^{GCKD}, and SIK3^{GCKD} animals. Error bars represent the mean +/- SEM. Statistical significance was determined by one-way ANOVA. (b) Unstimulated reproductive-age (6-8 weeks old) mice were sacrificed on the anticipated day of estrus, and oocytes were counted in the ampulla of each oviduct. The total number of oocytes ovulated by each animal is shown for WT and SIK2 global knockout (SIK2^{KO}) animals. Error bars represent the mean +/- SEM. Statistical significance was determined by Student's *t*-test. *P<0.05; ***P<0.001 vs. controls. (c) Representative H&E-stained ovary sections from prepubertal WT, SIK2^{GCKD}, and SIK3^{GCKD} mice treated with eCG for 48 h. Ovaries were imaged with 20X objective, scale bar = 700 µm. *P<0.05; ***P<0.001 vs. controls.

In contrast, SIK3^{GCKD} mice ovulated significantly fewer oocytes than controls in response to superovulation (Figure 5A), in concordance with the significantly smaller litter sizes of SIK3^{GCKD} animals (Figure 2A). To determine how the knockdown of SIK3 in GCs affected follicle development, resulting in a decrease in the number of ovulated oocytes, we evaluated and counted the follicles at different stages of development in superovulated ovaries (Figure 6). This

experiment revealed that SIK3^{GCKO} ovaries contained significantly more preantral follicles and significantly fewer corpora lutea than controls (Figure 6). The preantral stage precedes the gonadotropin-dependent development of the fluid-filled antrum. Therefore, SIK3 expression in the GCs is essential for the preantral-to-antral transition.

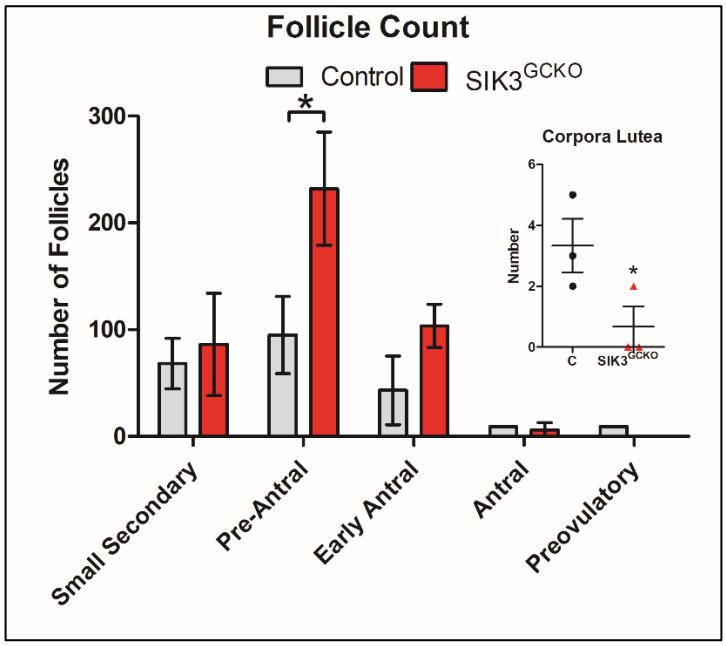

Figure 6. Loss of SIK3 in GCs disrupts folliculogenesis. Prepubertal (21-30 days old) mice were stimulated with 5 IU eCG for 48 h followed by 5 IU hCG for 17 h. Thereafter, ovaries were fixed, serially sectioned, and stained with H&E, then follicles were counted by follicle stage. The total number of secondary, pre-antral, early antral, antral, preovulatory follicles, and corpora lutea from one ovary per animal was calculated for controls and SIK3^{GCKD} mice. Values are displayed as the mean +/- SEM. Statistical significance was determined by two-way ANOVA for follicles and by Student's *t*-test for corpora lutea. *P<0.05 vs. controls.

As SIK2^{GCKD} and SIK3^{GCKD} mice showed alterations in folliculogenesis, which may be due to influences on GC proliferation or follicle atresia, we next investigated whether the loss of SIK2 and SIK3 in GCs affects proliferation and follicle survival. Ovaries from eCG-stimulated animals were subjected to immunohistochemistry to measure the expression of proliferating cell nuclear antigen (PCNA), a marker of proliferation, and cleaved caspase-3, a marker of apoptosis (Figure 7). Confirming results presented in Figure 5, histology examination suggests that SIK2^{GCKD} ovaries had more antral follicles than controls, while SIK3^{GCKD} ovaries appear to have fewer antral follicles and more secondary and preantral follicles than controls (Figure 7). Proliferation and apoptosis quantification revealed that SIK3^{GCKD} ovaries had significantly less PCNA-positive and more cleaved caspase 3-positive GCs than controls and SIK2^{GCKD} ovaries. Thus, SIK3 may regulate both the follicle growth and survival necessary to grow past the preantral stage.

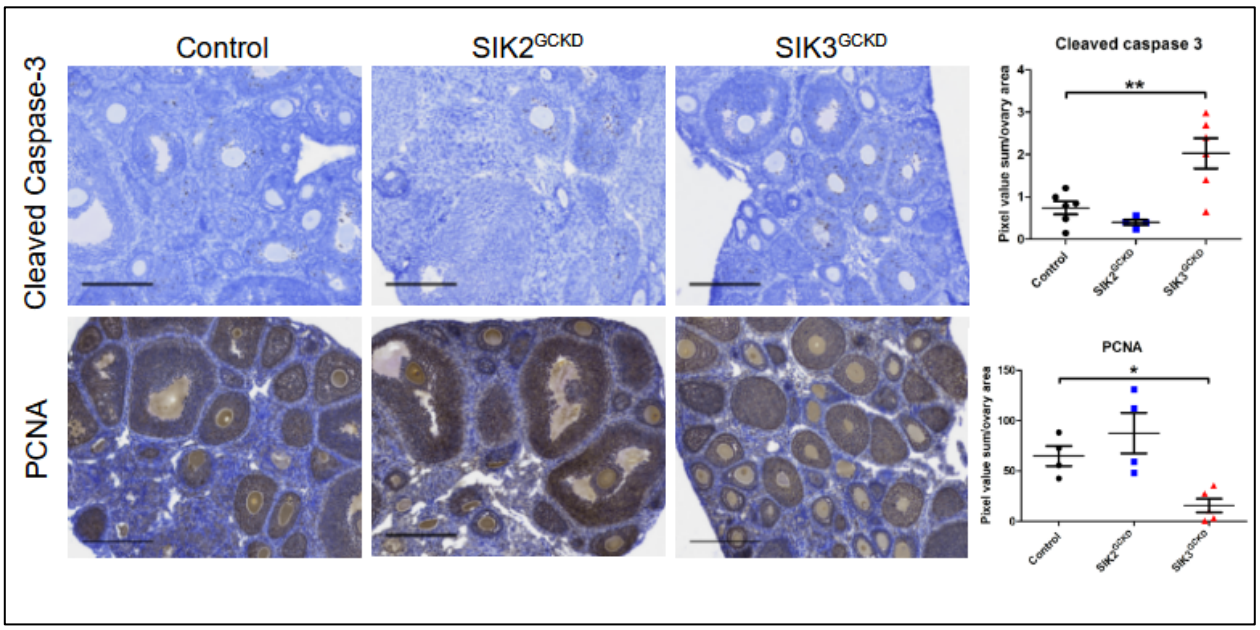

Figure 7. SIK2 and SIK3 in GCs differentially affect markers of proliferation and apoptosis. Prepubertal (21-30 days old) mice were stimulated with 5 IU eCG for 48 h, then ovaries were harvested, fixed, and used for IHC studies to detect cleaved caspase 3 (apoptosis marker) and PCNA (proliferation marker). Representative 10X images of wild-type control (Control), SIK2^{GCKD}, and SIK3^{GCKD} ovaries are displayed for cleaved caspase-3 (top) and PCNA (bottom). Brown coloring represents positive staining against blue hematoxylin counterstain. Quantification was performed by measuring the sum of positive pixels and dividing by the area of the ovary (right). Scale bar = 300 μm. Statistical significance was determined by one-way ANOVA. *P<0.05, **P<0.01 vs. controls.

DISCUSSION

The GCs are the somatic cells of the ovarian follicle that proliferate, participate in steroidogenesis, and nurture the oocyte. In particular, during the latter half of folliculogenesis, GC function is mainly controlled by gonadotropins, namely FSH, which triggers signaling pathways downstream of the FSHR and promotes GC proliferation and thus follicle progression, terminal differentiation, and survival. In this work, SIK2 and SIK3 showed differential regulation of steroidogenesis (Figure 3 and Figure 4)—a hallmark of GC terminal differentiation—and apoptosis (Figure 7). Further, SIK2 and SIK3 promoted and inhibited follicle growth, respectively; eCG-stimulated SIK2^{GCKD} animals ovulated significantly more oocytes (Figure 5A), while SIK3^{GCKD} ovulated fewer oocytes (Figure 5A) and had ovaries with more follicles stalled at the preantral stage (Figure 6). Thus, SIK2 and SIK3 mediate the effects of FSH in GCs *in vivo* in opposite ways.

The specific mechanisms by which the SIKs act in GCs require further elucidation. The canonical pathway downstream of the Gs-coupled protein receptor FSHR is the cAMP-PKA-CREB pathway, in which CREB is the transcription factor promoting the expression of steroidogenic enzymes. One family of targets of SIK phosphorylation is the CREB-regulated transcriptional coactivators (CRTCs). Interestingly, our group recently showed that SIK inhibition and FSH stimulation in rat GCs *in vitro* promote nuclear localization of CRTC2 [10]. Moreover,

we showed that SIK inhibition does not affect PKA or CREB phosphorylation, suggesting that the SIKs act downstream of CREB to affect CREB-mediated transcription [10]. Thus, CRTC2 may be regulated by SIKs in GCs *in vitro* and *in vivo*. In our $SIK2^{GCKD}$ mice, we saw increased serum estradiol and steroidogenic gene expression (Figure 3 and Figure 4), consistent with our previous work in rat and human GCs *in vitro* [9,10]. Therefore, steroidogenesis may be regulated via an FSH-SIK2-CRTC2 pathway that augments CREB activity in the nucleus. However, further experimentation is required to establish this pathway in the ovary.

In addition to promoting steroidogenesis, the $SIK2^{GCKD}$ mice ovulated significantly more oocytes than wild-type controls, recapitulating the hyper-response to superovulation seen in the SIK2 global knockout ($SIK2^{KO}$) mice [9] and demonstrating that SIK2 actions in the GCs mediate the effects of observed in the global knockout. Interestingly, compared to wild-type controls, the $SIK2^{GCKD}$ mice produced a similar number of pups over six months, and both $SIK2^{KO}$ and $SIK2^{GCKD}$ mice had similar litter sizes. We also determined that $SIK2^{KO}$ mice ovulate a similar number of oocytes without stimulation compared to wild-type animals [9]. Thus, this suggests that other mechanisms under physiology conditions may compensate for the loss of SIK2 but that this compensation may be overwhelmed by supraphysiologic doses of gonadotropins. These combined observations highlight SIK2 as a potential target for improving egg retrieval yield during controlled ovarian stimulation, an essential part of the *in vitro* fertilization process.

Though our previous and current work demonstrated that SIK inhibition and the loss of SIK2 in GCs and theca cells *in vitro* and *in vivo* promote steroidogenesis [9,10,17], $SIK3^{GCKD}$ mice showed significantly decreased levels of serum estradiol and significantly decreased steroidogenic gene expression (Figure 3 and Figure 4). Further, the $SIK3^{GCKD}$ ovaries showed growth defects and increased atretic follicles (Figures 6 and 7). Thus, it is unlikely that SIK3 signals via the CRTCs to mediate these effects. Another well-established target of the SIKs is the class IIa histone deacetylases (HDACs), which seem to mediate SIK3 effects on circadian rhythm, metabolism, and skeletal development [18–21]. It may be possible that SIK3 actions in GCs are mediated by class IIa HDACs. Other important signal transducers downstream of the FSHR are ERK1/2, which may mediate anti-apoptotic, proliferative, and steroidogenic effects, and Akt, which is also anti-apoptotic in GCs [22]. However, we have demonstrated that SIK activity inhibition in GCs does not affect FSH stimulation of ERK1/2 and AKT [10]. Interestingly, SIK inhibition decreases FBS-induced Akt phosphorylation in vascular smooth muscle cells, and this effect was attributed to SIK3 [23]. Thus, the evidence does not suggest that AKT or AKT may mediate the effect of SIK3, although this remains to be determined.

In considering SIK3 in the fertility regulation, we hypothesized that the loss of SIK3 in the GCs would recapitulate the infertile, gonadotropin-resistant phenotype seen in SIK3 global knockout mice [9]. However, the $SIK3^{GCKD}$ animals in this study produced litters, though they accumulated significantly fewer pups than WT controls over six months (Figure 2). There are three possibilities for why the $SIK3^{GCKD}$ animals were subfertile but not infertile. First, the $SIK3^{GCKD}$ GCs showed a significant knockdown but not a knockout of SIK3 (Figure 1). Thus, it is possible that low but not absent SIK3 in the GCs may preserve fertility. Second, SIK3 may have essential roles in the GCs prior to or during differentiation. Our experimental approach utilized the CYP19A1 proximal promoter II to drive Cre recombinase expression, thus requiring gonadotropin stimulation for Cre recombinase expression and thereby initiating differentiation [13]. And third, SIK3 may have important fertility regulatory actions in the theca cells and the oocyte. Previously, our group showed that SIK3 is the most abundant SIK expressed in the theca cells and that broad SIK inhibition using the small molecule inhibitor HG-9-91-01 regulates androgen synthesis in theca cells [17]. In the oocyte, the critical activator of SIK kinase activity, liver kinase B1 (LKB1, also known as STK11), has been shown to regulate primordial follicle

activation; oocyte-specific knockout of LKB1 in a mouse model promotes premature ovarian failure [24]. Thus, it is plausible that SIK3 may be involved in theca cell and oocyte function, though further work is required to determine whether SIK3 regulates fertility via actions in the other follicle components. Regardless, illuminating the follicle-attenuating role of SIK3 in the GCs supports the potential of targeting the SIK3 pathway as a non-hormonal strategy for contraception.

In conclusion, we showed that SIK2 and SIK3 play opposite *in vivo* roles in regulating GC function, follicle development, and—in the case of SIK3—fertility. Together, our findings contribute to a better understanding of the *in vivo* role of SIKs in female fertility. Further, this work hopes to inform future studies investigating the role of the SIKs in reproductive pathophysiology as well as the potential of the SIKs as therapeutic targets for treating infertility and developing new contraceptives.

REFERENCES

[1] Cox CM, Thoma ME, Tchangalova N, Mburu G, Bornstein MJ, Johnson CL, Kiarie J. Infertility prevalence and the methods of estimation from 1990 to 2021: a systematic review and meta-analysis. Human Reproduction Open 2022; 2022:hoac051.

[2] Carson SA, Kallen AN. Diagnosis and Management of Infertility: A Review. JAMA 2021; 326:65.

[3] Orisaka M, Miyazaki Y, Shirafuji A, Tamamura C, Tsuyoshi H, Tsang BK, Yoshida Y. The role of pituitary gonadotropins and intraovarian regulators in follicle development: A mini□ review. Reprod Medicine & Biology 2021; 20:169–175.

[4] Saint□Dizier M, Malandain E, Thoumire S, Remy B, Chastant□Maillard S. Expression of follicle stimulating hormone and luteinizing hormone receptors during follicular growth in the domestic cat ovary. Molecular Reproduction Devel 2007; 74:989–996.

[5] Simoni M, Gromoll J, Nieschlag E. The Follicle-Stimulating Hormone Receptor: Biochemistry, Molecular Biology, Physiology, and Pathophysiology*. Endocrine Reviews 1997; 18:739–773.

[6] Szkudlinski MW. New Frontier in Glycoprotein Hormones and Their Receptors Structure–Function. Front Endocrinol 2015; 6.

[7] Themmen APN, Huhtaniemi IT. Mutations of Gonadotropins and Gonadotropin Receptors: Elucidating the Physiology and Pathophysiology of Pituitary-Gonadal Function. Endocrine Reviews 2000; 21:551–583.

[8] Darling NJ, Cohen P. Nuts and bolts of the salt-inducible kinases (SIKs). Biochemical Journal 2021; 478:1377–1397.

[9] Armouti M, Winston N, Hatano O, Hobeika E, Hirshfeld-Cytron J, Liebermann J, Takemori H, Stocco C. Salt-inducible Kinases Are Critical Determinants of Female Fertility. Endocrinology 2020; 161:bqaa069.

[10] Armouti M, Rodriguez-Esquivel M, Stocco C. Mechanism of negative modulation of FSH signaling by salt-inducible kinases in rat GCs. Front Endocrinol 2022; 13:1026358.

[11] Patel K, Foretz M, Marion A, Campbell DG, Gourlay R, Boudaba N, Tournier E, Titchenell P, Peggie M, Deak M, Wan M, Kaestner KH, et al. The LKB1-salt-inducible kinase pathway functions as a key gluconeogenic suppressor in the liver. Nat Commun 2014; 5:4535.

[12] Yahara Y, Takemori H, Okada M, Kosai A, Yamashita A, Kobayashi T, Fujita K, Itoh Y, Nakamura M, Fuchino H, Kawahara N, Fukui N, et al. Pterosin B prevents chondrocyte hypertrophy and osteoarthritis in mice by inhibiting Sik3. Nat Commun 2016; 7:10959.

[13] Fan H-Y, Shimada M, Liu Z, Cahill N, Noma N, Wu Y, Gossen J, Richards JS. Selective expression of *KrasG12D* in GCs of the mouse ovary causes defects in follicle development and ovulation. Development 2008; 135:2127–2137.

[14] Ajayi AF, Akhigbe RE. Staging of the estrous cycle and induction of estrus in experimental rodents: an update. Fertil Res and Pract 2020; 6:5.

[15] Bingel AS, Schwartz NB. TIMING OF LH RELEASE AND OVULATION IN THE CYCLIC MOUSE. Reproduction 1969; 19:223–229.

[16] Pedersen T, Peters H. PROPOSAL FOR A CLASSIFICATION OF OOCYTES AND FOLLICLES IN THE MOUSE OVARY. Reproduction 1968; 17:555–557.

[17] Rodriguez Esquivel M, Hayes E, Lakomy O, Hassan M, Foretz M, Stocco C. Salt-inducible kinases regulate androgen synthesis in theca cells by enhancing CREB signaling. Molecular and Cellular Endocrinology 2023:112030.

[18] Asano F, Kim SJ, Fujiyama T, Miyoshi C, Hotta-Hirashima N, Asama N, Iwasaki K, Kakizaki M, Mizuno S, Mieda M, Sugiyama F, Takahashi S, et al. SIK3–HDAC4 in the suprachiasmatic nucleus regulates the timing of arousal at the dark onset and circadian period in mice. Proc Natl Acad Sci USA 2023; 120:e2218209120.

[19] Fujii S, Emery P, Amrein H. SIK3–HDAC4 signaling regulates *Drosophila* circadian male sex drive rhythm via modulating the DN1 clock neurons. Proc Natl Acad Sci USA 2017; 114.
[20] Choi S, Lim D-S, Chung J. Feeding and Fasting Signals Converge on the LKB1-SIK3 Pathway to Regulate Lipid Metabolism in Drosophila. PLoS Genet 2015; 11:e1005263.
[21] Sasagawa S, Takemori H, Uebi T, Ikegami D, Hiramatsu K, Ikegawa S, Yoshikawa H, Tsumaki N. SIK3 is essential for chondrocyte hypertrophy during skeletal development in mice. Development 2012; 139:1153–1163.
[22] Casarini L, Crépieux P. Molecular Mechanisms of Action of FSH. Front Endocrinol 2019; 10:305.
[23] Cai Y, Wang X-L, Lu J, Lin X, Dong J, Guzman RJ. Salt-Inducible Kinase 3 Promotes Vascular Smooth Muscle Cell Proliferation and Arterial Restenosis by Regulating AKT and PKA-CREB Signaling. ATVB 2021; 41:2431–2451.
[24] Jiang Z-Z, Hu M-W, Ma X-S, Schatten H, Fan H-Y, Wang Z-B, Sun Q-Y. LKB1 acts as a critical gatekeeper of ovarian primordial follicle pool. Oncotarget 2016; 7:5738–5753.